ing activity. The GDP-releasing activity eluted as a single peak at an apparent molecular mass between 100,000 and 160,000 daltons (Fig. 3). However, because of the highly cooperative nature of the interaction between $p21^{ras}$ and Ras-GRF, it remains unclear whether this value represents the molecular size of the fully active factor.

We conclude that Ras-GRF is a novel protein, distinct from Ras-GAP, that enhances the off rate of guanine nucleotides from $p21^{ras}$. Although we do not yet understand the mechanisms that might regulate GDP-releasing activity, we observed that cytosol prepared in the absence of phosphatase inhibitors exhibited significantly less activity than that prepared in the presence of phospho-amino acids and *p*-nitrophenyl phosphate (Table 1). Moreover, the releasing activity did not remove all of the [α-^{32}P]GDP from Ras (Fig. 1), and the rate and extent of release were rather variable from preparation to preparation. These data suggest that the Ras-GRF is rapidly inactivated, perhaps by dephosphorylation, which might account for the difficulties others have encountered in trying to detect a GTP/GDP exchange activity for Ras.

Although it was surprising to detect Ras-GRF in the cytosol rather than associated with the plasma membrane, the result supports earlier suspicions that the Ras superfamily of proteins is structurally and functionally more closely related to factors involved in the control of vectorial processes such as EF-Tu and eIF-2, rather than to the trimeric G proteins (*10*). The guanine nucleotide-exchange factor for eIF-2 is a large cytosolic protein, the interaction of which with eIF-2 is governed by phosphorylation (*7*).

We therefore propose that Ras-GRF allows the rapid equilibration of $p21^{ras}$ with the free guanine nucleotide pools in the cell, to control the fraction of *ras* protein in the on state.

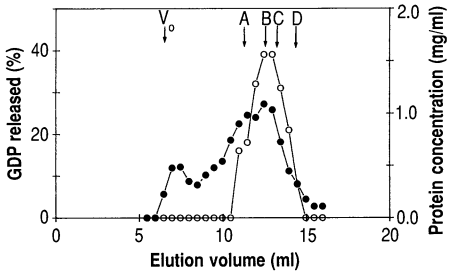

Fig. 3. Gel filtration chromatography of *ras*-GRF. Rat brain cytosol was concentrated in a Centricon 10 (approximately fivefold) and loaded onto a Superose 12 sizing column (5 mg in 0.1 ml). The column was eluted with 20 m*M* tris-HCl, *p*H 7.4, 125 m*M* NaCl, 10% glycerol, 1 m*M* $MgCl_2$, 1 m*M* DTT, plus phosphatase inhibitors (*8*). Fractions (0.5 ml) were assayed for GDP-releasing activity (open circles) as described in Fig. 1. Protein (closed circles) was measured by a modification of the method described by Lowry (*14*). The column was calibrated with (A) amylase (200 kD), (B) alcohol dehydrogenase (150 kD), (C) bovine serum albumin (66 kD), and (D) carbonic anhydrase (29 kD). The results are representative of two independent experiments. V_0, void volume.

REFERENCES AND NOTES

1. M. Barbacid, *Annu. Rev. Biochem.* **56**, 779 (1987).
2. M. Trahey and F. McCormick, *Science* **238**, 542 (1987); J. Field, D. Broek, T. Tataoka, M. Wigler, *Mol. Cell. Biol.* 7, 2128 (1987).
3. F. McCormick, *Cell* **56**, 5 (1989); U. S. Vogel *et al.*, *Nature* **335**, 90 (1988); H. Adari, D. R. Lowy, B. M. Willumsen, C. J. Der, F. McCormick, *Science* **240**, 518 (1988).
4. A. Hall and A. J. Self, *J. Biol. Chem.* **261**, 10963 (1986); J. Feuerstein, R. S. Goody, A. Wittinghofer, *J. Biol. Chem.* **262**, 8455 (1987); M. Poe, E. M. Scolnick, R. B. Stein, *ibid.* **260**, 3906 (1985).
5. L. C. Robinson, J. B. Gibbs, M. S. Marshall, I. S. Sigal, K. Tatchell, *Science* **235**, 1218 (1987); D. Broek *et al.*, *Cell* **48**, 789 (1987).
6. P. J. Casey and A. G. Gilman, *J. Biol. Chem.* **263**, 2577 (1988); A. M. Speigel, *Mol. Cell. Endocrinol.* **49**, 1 (1987).
7. R. Panniers, A. G. Rowlands, E. C. Henshaw, *J. Biol. Chem.* **263**, 5519 (1988); A. G. Rowlands, R. Panniers, E. C. Henshaw, *ibid.*, p. 5526
8. Rat brains were homogenized at 4°C in a Waring blender, then with a Dounce homogenizer, in 20 m*M* 2-(*N*-morpholino)propanesulfonic acid (MOPS), *p*H 7.2, 1 m*M* $MgCl_2$, 0.1 m*M* EDTA, 1 m*M* dithiothreitol (DTT), 200 m*M* sucrose, plus aprotinin and leupeptin (25 μg/ml each), phenylmethylsulfonyl fluoride (PMSF) (40 μg/ml), and pepstatin A (1.7 μg/ml) as protease inhibitors, plus 1.5 m*M* *p*-nitrophenyl phosphate, 0.5 m*M* phosphoserine, 0.5 m*M* phosphotyrosine, and 1 m*M* phosphothreonine as phosphatase inhibitors. The homogenates were centrifuged at 100,000*g* for 30 min. The supernatants were used immediately.
9. J. Tucker *et al.*, *EMBO J.* **5**, 1351 (1986). Ras proteins were purified from 6-liter cultures of *E. coli*, by ammonium sulfate precipitation, a DE52 anion-exchange column, and Superose 12 size exclusion chromatography (Pharmacia FPLC). Glycerol (10%) was added to all chromatography buffers to stabilize the proteins.
10. A. Wolfman, A. Moscucci, I. G. Macara, *J. Biol. Chem.* **264**, 10820 (1989). Ras was loaded with [α-^{32}P]GDP (2 μCi/pmol) in the presence of 1 m*M* EDTA at 4°C for 30 min. The binary complex was then stabilized by the addition of 10 m*M* Mg^{2+}.
11. A. Wolfman and I. G. Macara, unpublished observations.
12. N. Ohga, A. Kikuchi, T. Ueda, J. Yamamoto, Y. Takai, *Biochem. Biophys. Res. Comm.* **163**, 1523 (1989).
13. The $p25^{rab3A}$ protein was purified to homogeneity from bovine brain as described previously [E. Burstein and I. G. Macara, *Mol. Cell. Biol.* **9**, 4807 (1989)].
14. O. Lowry, N. Rosenbrough, A. Farr, R. Randall, *J. Biol. Chem.* **193**, 265 (1951). To 100-μl samples, 1% deoxycholate (100 μl) and 10% trichloroacetic acid (1 ml) were added. After 10 min (at 4°C), samples were centrifuged in a microfuge for 5 min. The pellets were assayed for protein as described.

15. We thank A. Wittinghofer for kindly providing the ptacras vectors, D. Okuhara and V. Stathopoulos for purification of the H-Ras proteins, F. McCormick for providing recombinant Ras-GAP, and E. Henshaw and R. Panniers for their helpful suggestions for assaying Ras-GRF and the gift of purified GEF, and J. Wolfman for the protocol using sucrose cushions to isolate immuno-complexes. This work was supported by National Institute of Environmental Health Sciences Center grant ES 01247 and by NIH grants CA 43551 (to I.G.M.) and GM 41220 (to A.W.).

26 October 1989; accepted 31 January 1990

Characterization of an Extremely Large, Ligand-Induced Conformational Change in Plasminogen

WALTER F. MANGEL, BOHAI LIN,* V. RAMAKRISHNAN†

Native human plasminogen has a radius of gyration of 39 angstroms. Upon occupation of a weak lysine binding site, the radius of gyration increases to 56 angstroms, an extremely large ligand-induced conformational change. There are no intermediate conformational states between the closed and open form. The conformational change is not accompanied by a change in secondary structure, hence the closed conformation is formed by interaction between domains that is abolished upon conversion to the open form. This reversible change in conformation, in which the shape of the protein changes from that best described by a prolate ellipsoid to a flexible structure best described by a Debye random coil, is physiologically relevant because a weak lysine binding site regulates the activation of plasminogen.

NATIVE HUMAN PLASMINOGEN IS A single-chain polypeptide of 790 amino acids (*1*) located within six domains (*2*). At the NH_2-terminus are five kringles, triple-loop structures of 80 to 100 amino acids constrained by three disulfide bridges, followed by the protease domain which is homologous to chymotrypsin. The kringles have a high degree of sequence similarity (35%) and are autonomous structural and folding domains (*3*) that have evolved by exon shuffling (*4*). Plasmin is formed upon cleavage by a plasminogen activator of the arginyl-valyl bond 560 amino acids from the NH_2-terminus of plasminogen (*5*). There are two classes of lysine binding sites on plasminogen. For the ligand 6-aminohexanoic acid (6-AHA) there is

one strong site with a dissociation constant K_d of 9 μM and five weaker sites with a K_d of 5 mM (*6*). Plasminogen is targeted by way of the lysine binding sites. It is through the strong site in kringle 1 that plasminogen binds to fibrin (*7*), the extracellular matrix (*8*), and the cell surface (*9*). Occupation of the strong lysine binding site protects plasmin from its major inhibitor α_2-antiplasmin (*10*). Activation of plasminogen is regulated by the lysine binding sites. In the presence of 6-AHA sufficient to saturate a weak lysine binding site, the rate of activation by urokinase increases tenfold (*11*). Occupation of a weak lysine binding site by 6-AHA alters some of the physical properties of plasminogen (*6*). There is a reversible decrease in the sedimentation coefficient (*12*) from 5.75 to 4.85*S* (*13*), an increase of 7% in the intrinsic fluorescence, and a decrease in the rotational relaxation time from 262 to 158 ns (*14*).

Although a change in the conformation of plasminogen was known to occur upon occupation of a weak lysine binding site, the nature of this change and the precise physical dimensions involved were unknown. Our objective was to characterize the conformation of plasminogen in solution and the changes that occur upon occupation of the lysine binding sites. Small-angle scattering was chosen because it can be used to study directly and precisely conformational changes that occur in proteins in solution. Analysis of the low-angle part of the scattered intensity yields the radius of gyration (R_g) and the molecular weight without using any assumptions, whereas the data at higher angles can be used to estimate the approximate shape of the molecule (*15*). Vacuum ultraviolet circular dichroism (CD) can be used to estimate the secondary-structure content of proteins (*16*).

For small-angle neutron scattering, the intensity at very small angles obeys the Guinier relation (*17*). Guinier plots of the scattering data obtained with plasminogen in the presence and absence of 50 mM 6-AHA, both in H_2O and D_2O are shown in Fig. 1. Molecular weights are most accurately determined from the intercept of a Guinier plot for data collected in H_2O because the data in H_2O are relatively insensitive to partial specific volume. For plasminogen in the presence and absence of 6-AHA, a molecular weight of 94,000 was calculated, which agrees with reported values. The R_g is most accurately measured in D_2O from the slope of a Guinier plot. Native plasminogen had an R_g of 39.0 Å in D_2O. In the presence of 50 mM 6-AHA, the R_g increased to 56.1 Å.

This massive conformational change we observed was unprecedented and prompted us to perform numerous control experiments. Small-angle neutron scattering experiments were performed at several concentrations of plasminogen in H_2O and D_2O. There was no dependence of R_g or $I(0)$, the scattering intensity at zero angle, on protein concentration within the range studied (1 to 10 mg/ml). Thus any interparticle effects at very low scattering vector k did not measurably influence the slopes of the linear regions of the Guinier plots or the intercepts. After each experiment, the plasminogen was analyzed by SDS-PAGE under reducing conditions (*18*) and by polyacrylamide gel electrophoresis at *p*H 3.2 in urea (*19*), which indicated the presence of intact, native Glu-plasminogen.

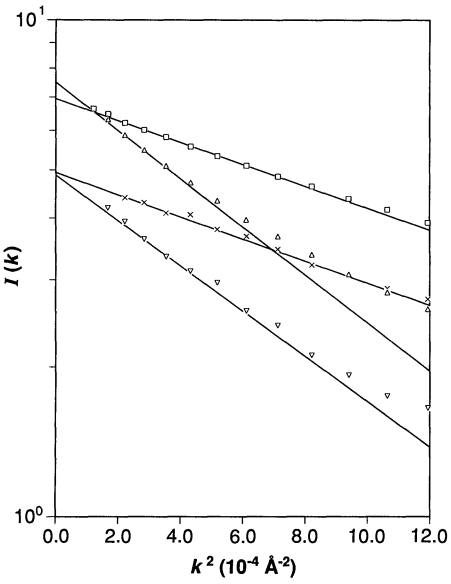

Fig. 1. Guinier plots {ln[$I(k)$] versus k^2} of the low-angle scattering from plasminogen with and without 6-AHA. $I(k)$ is the scattered intensity as a function of $k = 4\pi\sin\Theta/\lambda$, where 2Θ is the scattering angle and λ is the mean wavelength. Scattering in H_2O, (×) without and (▽) with 50 mM 6-AHA; scattering in D_2O, (□) without and with (△) 50 mM 6-AHA. Human plasminogen was purified and characterized as previously described (*33*). All small-angle scattering experiments were performed in Hepes-buffered saline (HBS), which contained 10 mM Hepes, *p*H 7.2, 0.137M NaCl, 2.68 mM KCl, 0.91 mM $CaCl_2$, and 0.49 mM $MgCl_2$. Prior to each experiment, plasminogen was fractionated on a Sephacryl 200 column in HBS to remove possible aggregates and then concentrated by filtration under nitrogen pressure over an Amicon PM-10 ultrafiltration membrane. For those experiments in D_2O, concentrated protein was dialyzed for 15 hours, with one change of buffer, against a 50-fold volume of HBS made up with D_2O. Small-angle neutron scattering measurements were done on the H9B spectrometer (*34*) in the High Flux Beam Reactor at Brookhaven National Laboratory. The mean incident wavelength varied, depending upon the experiment, from 4.5 to 7.5 Å. Protein samples and corresponding buffers were loaded into cylindrical quartz cells with a 1-mm path length for samples, 5 to 10 mg/ml, in H_2O and a 4-mm path length for samples, 1 to 5 mg/ml, in D_2O. All measurements were performed at 4°C. For data analysis, the scattered intensity was radially averaged and corrected for buffer and background scattering and then normalized for beam intensity, thickness, transmission, and protein concentration. The radius of gyration and forward scatter were estimated from a least-squares fit to the linear portion of Guinier plots of the data, using the equation $I(k) = I(0)\exp(-k^2R_g^2/3)$. The molecular weight was estimated from $I(0)$ for plasminogen in H_2O (*35*).

To determine whether there are conformations of plasminogen between that in the closed and open forms, we analyzed the titration curves. The dashed line in Fig. 2B is the scattering curve measured with all of the plasminogen in the closed form and the dotted line with all of it in the open form. The circles in Fig. 2B are the data points obtained from Fig. 2A at 2 mM 6-AHA. The solid line represents the best fit to these data points of a linear combination of closed and open forms. Since that line fits the data well, the scattering curve obtained in 2 mM 6-AHA is a superposition of the scattering curves for fully closed and open forms. Similar fits were obtained with the data in Fig. 2A acquired in 0.9 and 3 mM 6-AHA. The simplest conclusion from this analysis is that there are no intermediate conformations between the closed and open forms. Consistent with this conclusion is the single isobestic point in the titration curves in Fig. 2A.

The maximum dimensions of the closed and open forms of plasminogen were estimated by using the length distribution function, $P(r)$, which describes the distribution of distances between pairs of points in a particle (*20*). The function $P(r)dr$, the probability that two points in a particle are at a distance between r and $r + dr$, was determined by an indirect Fourier transformation (Fig. 3). For the closed form of plasminogen, the maximum dimension was 150 Å, whereas in the presence of 50 mM 6-AHA, $P(r) = 0$ at 240 Å.

W. F. Mangel and B. Lin, Biology Department, Brookhaven National Laboratory, Upton, NY 11973.
V. Ramakrishnan, Center for Structural Biology, Biology Department, Brookhaven National Laboratory, Upton, NY 11973.

*Present address: Institute of Biophysics, Academia Sinica, Beijing, China.
†To whom correspondence should be addressed.

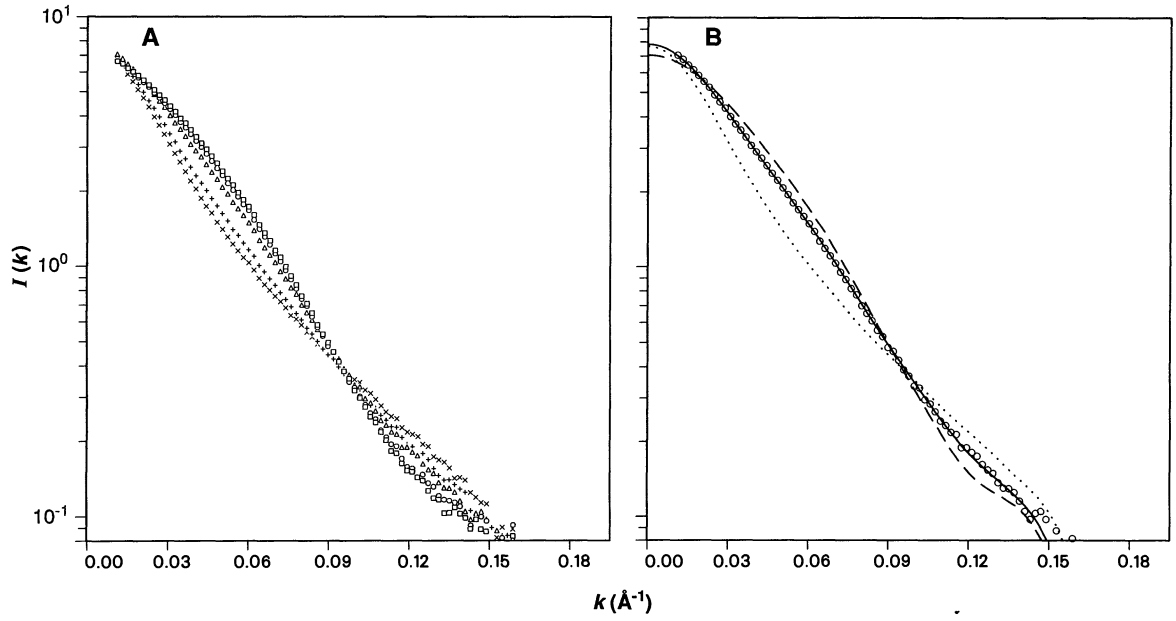

Fig. 2. (**A**) Titration of plasminogen with 6-AHA. Scattering curves of plasminogen in the presence of 0.5 (□), 0.9 (○), 2 (△), 3 (+), and 5 (×) m*M* 6-AHA. (**B**) Scattering of plasminogen in 2 m*M* 6-AHA (circles) expressed as a linear combination of the scattering from the closed (dashed line) and open (dotted line) forms of plasminogen. The solid line shows the best fit.

The shape of a molecule and its internal structure is reflected in the higher angle scattering intensity (*15*). An estimate of the shape of the closed and open forms of plasminogen can be obtained by model-building in which the objective is to find the shape of uniform scattering length density whose calculated scatter most closely matches the experimentally derived scatter. The shapes tested were a sphere, cylinder, ellipsoids of revolution, and a Debye random coil (*21*). The main physical difference between a Debye random coil and a highly elongated cylinder or ellipsoid is that the Debye random coil represents an average of an ensemble of many different conformations arising from flexibility. All of the parameters including the radius of gyration were allowed to float, and the results are summarized in Table 1. The best fit to the higher angle plasminogen scattering data collected in the absence of 6-AHA was from a prolate ellipsoid with dimensions of 147 Å by 57 Å (Fig. 4A). The shoulder in the curve which begins at (0.13 Å^{-1}) probably arises from interference between characteristic interdomain spacings. The higher angle scattering curve of the open form did not fit at all well to regular solids even in the low-angle range $k = 0$ to 0.10 Å^{-1}, where a prolate ellipsoid gave a good fit to the closed form. An excellent fit for the open form of plasminogen was from a Debye random coil (Fig. 4B). The shoulder in Fig. 4A is not present in Fig. 4B, which is consistent with the interdomain spacings of the open form of plasminogen being no longer fixed, as a result of flexibility.

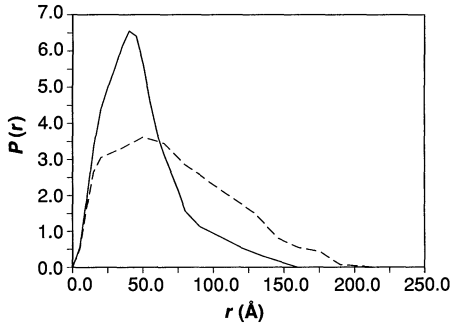

Fig. 3. Length distribution function of the scattering of plasminogen without (solid line) and with (dashed line) 50 m*M* 6-AHA.

Table 1. Physical parameters of native human plasminogen in the presence (+) and absence (−) of 6-aminohexanoic acid (6-AHA).

Parameter	(−) 6-AHA	(+) 6-AHA
Radius of gyration (Å)	39.0 ± 0.6	56.1 ± 1.1
Maximum dimension (Å)	150	240*
Shape	Prolate ellipsoid	Debye coil
Axial ratio	2.6	>5

*Average maximum dimension of ensemble of conformations.

Although the shape of plasminogen changed dramatically in the presence of 6-AHA, the secondary structure, as determined by CD spectroscopy, did not change. The spectra for plasminogen in the presence and absence of 50 m*M* 6-AHA were virtually superimposable (Fig. 5). These data were analyzed by a method that uses inverse CD spectra for each of the five major secondary structures of proteins (*16*). The method predicts the fraction of each secondary structure by forming the dot product of the corresponding inverse CD spectrum, expressed as a vector, with the CD spectrum of the protein. Plasminogen in either the open or closed form contained little or no α-helix or parallel β-sheet (Table 2). Most of the secondary structure was in the form of antiparallel β-sheet and β-turns. As controls, we obtained the CD spectra of chymotrypsin in the presence and absence of 50 m*M* 6-AHA (Table 2). The results were analyzed by the same method and compared favorably to the secondary structure of chymotrypsin determined by x-ray crystallography.

An important conclusion from the CD experiments is that the secondary structure of plasminogen does not change upon conversion from the closed to the open form. Since that structure must lie within the six domains, that is, the five kringles and the protease domain, the structure within the domains must not change upon conversion from the closed to the open form. This indicates that the shape of native plasminogen is formed by domain interaction and that this is abolished upon conversion to the open form. Our conclusions on the secondary structure of plasminogen are different from those obtained in a much earlier report (*22*). Our spectra were obtained down to 178 nm as opposed to 200 nm. Although spectra measured down to 200 nm can be used to determine accurately the amount of α-helix in a protein, they cannot be used to solve for other structures (*23*). The secondary structure of plasminogen using statistical methods of Chou and Fasman yielded 12% α-helix, 32% β-sheet, 35% β-turn, and 19% coil, a result somewhat similar to ours (*24*). An indication that our results are reliable is the absence of large, negative fractions of structure and that the sum of structure is near 100% (*16*).

Our data on the shapes of plasminogen are internally consistent. A large change in R_g but no change in $I(0)$ implies that a large conformational change has occurred rather

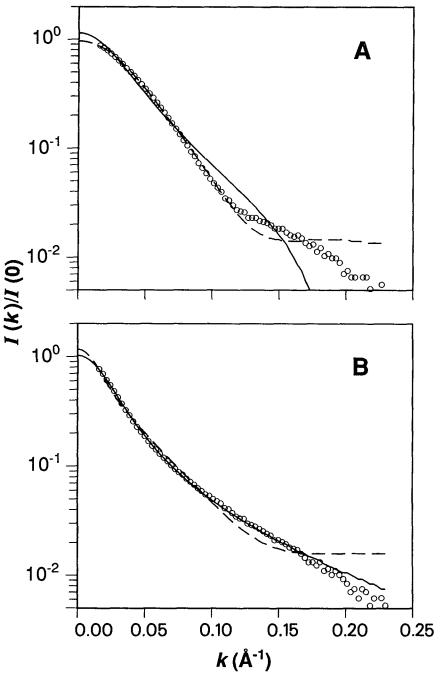

Fig. 4. Comparison of the higher angle scattering data of plasminogen to model structures. The models are a prolate ellipsoid (dashed line) and a Debye random coil (solid line). Plasminogen in the absence (**A**) and in the presence (**B**) of 50 m*M* 6-AHA. Shape analysis was performed by fitting the entire scattering curve to model functions for spheres, ellipsoids of revolution, cylinders, and Debye random coils. Only the data collected in D_2O buffers were used for shape analysis, because they have a much better signal to noise ratio due to the lower incoherent scattering of D_2O compared with H_2O.

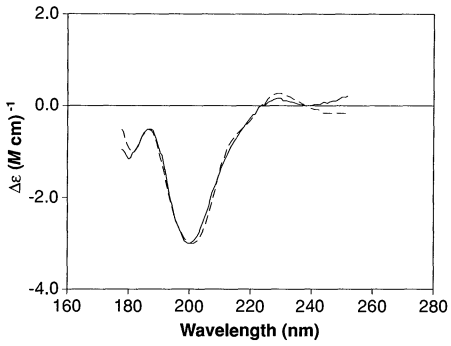

Fig. 5. Vacuum ultraviolet CD spectrum of plasminogen without (solid line) and with (dashed line) 50 m*M* 6-AHA. Measurements were made using the vacuum spectrometer U9B of the National Synchrotron Light Source at Brookhaven National Laboratory (*36*). Experiments were performed at room temperature in a quartz cell with a 12.5-μm path at a protein concentration of 5 mg/ml in HBS. The CD signals are expressed as the differences in the molar extinction coefficient $\Delta\epsilon$ of the left (ϵ_L)– and right (ϵ_R)–handed components of circularly polarized light as a function of wavelength.

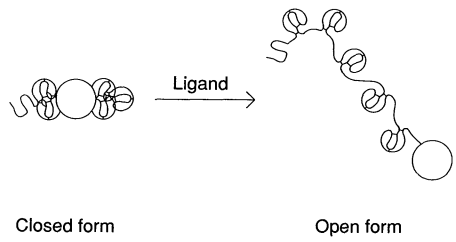

Fig. 6. A two-dimensional sketch of the conformational change in plasminogen induced upon occupation of a weak lysine binding site by the ligand 6-AHA. In the absence of ligand, the domains in plasminogen interact to form a molecule with the overall shape of a prolate ellipsoid with dimensions of 147 Å by 57 Å by 57 Å. Binding of the ligand converts this into an extended flexible structure in which the interaction between the domains is abolished. Three disulfide bridges are shown in each of the five kringles and the circle represents the protease domain. The closed and open forms are drawn to scale.

than aggregation. The small but reproducible change in $I(0)$ in Fig. 1 for the samples in D_2O but not in H_2O, implies that this conformational change is accompanied by a change in partial specific volume. If the partial specific volume for the open form is 0.75 cm^3/g based upon amino acid composition, the data indicate the partial specific volume for the closed form is 0.72 cm^3/g. For the shape analysis from the higher angle scattering data obtained in D_2O, all of the variables were allowed to float. The best fit for the closed form, to a prolate ellipsoid with dimensions of 147 Å by 57 Å by 57 Å, is consistent with the R_g independently determined from the Guinier plot to be 39 Å and with the maximum dimension independently determined from the $P(r)$ curve to be 150 Å. The best fit for the open form, to a Debye random coil, is evidence for a flexible structure. This does not mean that in the open form plasminogen is denatured, rather the regions between the domains have become flexible and the individual domains are no longer spatially constrained with respect to one another. Consistent with this is the increase in the maximum dimension determined from $P(r)$, from 150 Å for the closed form to a mean of 240 Å for the open form. From the values of R_g, we estimate the sedimentation coefficients to be 5.4 and 4.6*S* in the closed and open forms, respectively (*25*), in good agreement with the observed values of 5.75 and 4.85*S* (*13*). The titration data indicate the K_d for conversion from the closed to the open form is about 2 m*M* 6-AHA, a value near that of 3.3 m*M* obtained as the midpoint in the change in sedimentation coefficient with increasing concentrations of 6-AHA (*26*).

Large changes in protein conformation upon ligand binding have been shown to occur mostly in oligomeric, allosteric proteins. Upon oxygenation of deoxyhemoglobin, the radius of gyration decreases from 26.2 to 24.7 Å (*27*). Similarly, conversion from inactive to active forms results in changes in R_g from 24.7 to 23.5 Å for hexokinase (*28*) and 23.3 to 22.2 Å for phosphoglycerate kinase (*29*). Plasminogen may represent the extreme, as its conformational change is almost an order of magnitude greater. Other characteristics of the closed and open forms of plasminogen are also reminiscent of the R and T (relaxed and tense) structures of allosteric proteins described by Monod, Wyman, and Changeux (*30*). The shape of the closed form is determined by noncovalent interactions between domains. Ligand binding to the closed forms causes a reversible conformational change to the open form. The affinities for ligands of the closed form are different than of the open form. There are two states, a relatively inactivatable, closed form and a more activatable, open form. Plasminogen may be viewed as an oligomeric, allosteric protein that, instead of consisting of six, single-chain polypeptides, consists of six domains in a single polypeptide connected by random coils. The transition from a closed form in which the domains interact to produce the overall shape of a prolate ellipsoid to an open form that is more flexible and extended is illustrated in Fig. 6.

The open form of plasminogen may be more readily activated than the closed form, because the increase in flexibility may facilitate the binding of urokinase, leading to the tenfold decrease in the Michaelis constant K_m so that it approaches the physiological

Table 2. Secondary structure of human plasminogen and of chymotrypsin (control) as determined by circular dichroism in presence (+) and absence (−) of 6-AHA.

	α-Helix (%)	Antiparallel β-sheet (%)	Parallel β-sheet (%)	β-Turns (%)	Other structure (%)
		Plasminogen			
(−) 6-AHA	2.7 ± 1.4	36 ± 4.4	−1.6 ± 3.2	28 ± 2.1	34 ± 2.5
(+) 6-AHA (50 m*M*)	3.6 ± 1.1	36 ± 3.9	−2.7 ± 1.8	29 ± 1.8	34 ± 2.7
		Chymotrypsin			
(−) 6-AHA	13	25	0	23	38
(+) 6-AHA (50 m*M*)	12	27	0	23	38
Calculated from x-ray structure	10	34	0	20	36

concentration of plasminogen (*31*). The flexibility of the open form of plasmin may be important in its role in fibrinolysis. Since plasmin binds to fibrin through kringle 1, the protease domain, 554 amino acids away at the opposite end of the molecule, has a large radius within which to cleave fibrin (*32*). This would allow the open form, Lys-plasmin, to act catalytically on fibrin whereas the more rigid closed form of plasmin may act only stoichiometrically. Preliminary analysis of small-angle neutron scattering data from a variant of plasminogen missing the first 76 amino acids, Lys-plasminogen, and an NH_2-terminal fragment of plasminogen containing the first 3 kringles, indicates that their conformations were in the open form in the presence or absence of ligand binding.

REFERENCES AND NOTES

1. P. Wallen and B. Wiman, *Biochem. Biophys. Acta* **257**, 122 (1972).
2. L. Sottrup-Jensen, H. Claeys, M. Zajdel, T. E. Peterson, S. Magnusson, *Prog. Chem. Fibrinolysis Thrombolysis* **3**, 191 (1978).
3. F. J. Castellino, V. A. Ploplis, J. R. Powell, D. K. Strickland, *J. Biol. Chem.* **256**, 4778 (1981); V. A. Ploplis, D. K. Strickland, F. J. Castellino, *Biochemistry* **20**, 15 (1981); V. V. Novokhatny, S. A. Kudinov, P. L. Privalov, *J. Mol. Biol.* **179**, 215 (1984); M. Trexler and L. Patthy, *Proc. Natl. Acad. Sci. U.S.A.* **80**, 2457 (1983).
4. L. Patthy, *Cell* **41**, 657 (1985).
5. K. C. Robbins, L. Summaria, B. Hsih, R. Shah, *J. Biol. Chem.* **242**, 2333 (1967).
6. G. Markus, J. L. De Pasquale, F. C. Wissler, *ibid.* **253**, 733 (1978).
7. S. Thorsen, *Biochim. Biophys. Acta* **251**, 363 (1975); E. Suenson and S. Thorsen, *Biochem. J.* **197**, 619 (1982); M. A. Lucas, L. J. Freeto, P. A. McKee, *J. Biol. Chem.* **258**, 4249 (1983); R. Bok and W. F. Mangel, *Biochemistry* **24**, 3279 (1985).
8. B. S. Knudsen, R. L. Silverstein, L. L. K. Leung, P. C. Harpel, R. L. Nachman, *Proc. Natl. Acad. Sci. U.S.A.* **261**, 10765 (1986).
9. E. F. Plow, D. E. Freaney, J. Plescia, L. A. Miles, *J. Cell Biol.* **103**, 2411 (1986).
10. B. Wiman and D. Collen, *Nature* **272**, 549 (1978).
11. U. Christensen and S. Mullertz, *Biochim. Biophys. Acta* **481**, 271 (1977); U. Christensen, *ibid.*, p. 638; S. W. Peltz, T. A. Hardt, W. F. Mangel, *Biochemistry* **21**, 2798 (1982).
12. N. Alkjaersig, *Biochem. J.* **93**, 171 (1964).
13. W. J. Brockway and F. J. Castellino, *Arch. Biochem. Biophys.* **151**, 494 (1972); B. N. Violand, R. Bryne, F. J. Castellino, *J. Biol. Chem.* **253**, 5395 (1978).
14. F. J. Castellino, W. J. Brockway, J. K. Thomas, H. Liao, A. B. Rawitch, *Biochemistry* **12**, 2787 (1973).
15. O. Glatter and O. Kratky, Eds., *Small Angle X-Ray Scattering* (Academic Press, London, 1982).
16. L. A. Compton and W. C. Johnson, Jr., *Anal. Biochem.* **155**, 155 (1986).
17. A. Guinier and B. Fournet, *Small Angle Scattering of X-Rays* (Wiley, New York, 1955).
18. U. K. Laemmli, *Nature* **227**, 680 (1972).
19. S. Panyim and R. Chalkley, *Arch. Biochem. Biophys.* **130**, 337 (1969).
20. P. B. Moore, *J. Appl. Cryst.* **13**, 168 (1980).
21. R. G. Kriste and R. C. Oberthur, in (*15*), pp. 387–432.
22. I. Sjoholm, B. Wiman, P. Wallen, *Eur. J. Biochem.* **39**, 471 (1973).
23. J. B. Siegel, W. E. Steinmetz, G. L. Long, *Anal. Biochem.* **104**, 160 (1980).
24. J. R. Powell, J. M. Beals, F. J. Castellino, *Arch. Biochem. Biophys.* **248**, 390 (1986).
25. T. F. Kumosinski and H. Pessen, *ibid.* **219**, 89 (1982).
26. G. Markus, J. L. Evers, G. H. Hobika, *J. Biol. Chem.* **253**, 733 (1978).
27. H. Conrad, A. Mayer, H. P. Thomas, H. Vogel, *J. Mol. Biol.* **41**, 225 (1969).
28. R. C. McDonald, T. A. Steitz, D. M. Engelman, *Biochemistry* **18**, 338 (1979).
29. C. A. Pickover, D. B. McKay, D. M. Engelman, T. A. Steitz, *J. Biol. Chem.* **254**, 11323 (1979).
30. J. Monod, J. Wyman, J. P. Changeux, *J. Mol. Biol.* **12**, 88 (1965).
31. S. W. Peltz, T. A. Hardt, W. F. Mangel, *Biochemistry* **21**, 2798 (1982).
32. V. Ramakrishnan, L. Patthy, W. F. Mangel, unpublished results.
33. D. C. Livingston *et al.*, *Biochemistry* **20**, 4298 (1981); S. P. Leytus *et al.*, *ibid.*, p. 4307; S. W. Peltz, T. A. Hardt, W. F. Mangel, *ibid.* **21**, 2798 (1982); L. L. Melhado, S. W. Peltz, S. P. Leytus, W. F. Mangel, *J. Am. Chem. Soc.* **104**, 7299 (1982); R. Bok and W. F. Mangel, *Biochemistry* **24**, 3279 (1985).
34. D. Schneider and B. P. Schoenborn, in *Neutrons in Biology*, B. P. Schoenborn, Ed. (Plenum, New York, 1984), pp. 119–142.
35. B. Jacrot and G. Zaccai, *Biopolymers* **20**, 2413 (1981).
36. J. C. Sutherland, E. J. Desmond, P. Z. Takacs, *Nucl. Instrum. Methods* **172**, 195 (1980); J. C. Sutherland, P. C. Keck, K. P. Griffin, P. Z. Takacs, *ibid.* **195**, 375 (1982).

37. We thank D. Schneider for help with the neutron scattering measurements, J. Sutherland for help with the circular dichroism measurements, and D. Toledo and J. Trunk for able technical assistance. This work was supported by the Office of Health and Environmental Research of the United States Department of Energy. The High Flux Beam Reactor and the National Synchrotron Light Source are supported by the Division of Chemical Sciences and the Division of Materials Sciences, Office of Basic Energy Sciences, United States Department of Energy.

13 November 1989; accepted 6 February 1990

Two-Photon Laser Scanning Fluorescence Microscopy

WINFRIED DENK,* JAMES H. STRICKLER, WATT W. WEBB

Molecular excitation by the simultaneous absorption of two photons provides intrinsic three-dimensional resolution in laser scanning fluorescence microscopy. The excitation of fluorophores having single-photon absorption in the ultraviolet with a stream of strongly focused subpicosecond pulses of red laser light has made possible fluorescence images of living cells and other microscopic objects. The fluorescence emission increased quadratically with the excitation intensity so that fluorescence and photobleaching were confined to the vicinity of the focal plane as expected for cooperative two-photon excitation. This technique also provides unprecedented capabilities for three-dimensional, spatially resolved photochemistry, particularly photolytic release of caged effector molecules.

WE REPORT THE APPLICATION OF two-photon excitation of fluorescence (*1*) to laser scanning microscopy (LSM) (*2*). In LSM, the laser is focused to a diffraction-limited beam waist <1 μm in diameter and is raster-scanned across a specimen. Confocal LSM provides depth discrimination and improves spatial resolution within the plane of focus by forming the image through the same scanning optics used for illumination and through a pinhole placed in front of the detector, which acts as a spatial filter to select emission from the plane of focus (*2*). Very good laser scanning micrographs have been obtained with the use of fluorescent markers that absorb and emit visible light (*3*). Confocal scanning images with fluorophores and fluorescent chemical indicators that are excited by the ultraviolet (UV) part of the spectrum have not appeared, however, largely because of the lack of suitable microscope lenses, which must be chromatically corrected and transparent for both absorption and emission wavelengths (*4, 5*). Anticipated photodamage to living cells and the limitations of UV lasers have also inhibited this approach.

Two-photon molecular excitation (*1, 6*) is made possible by the very high local instantaneous intensity provided by the tight focusing in an LSM combined with the temporal concentration of a femtosecond pulsed laser. With a colliding-pulse, mode-locked dye laser (*7*) (CPM) producing a stream of pulses with a pulse duration (τ_p) of about 100 fs at a repetition rate (f_p) of about 80 MHz, the probability becomes appreciable for a dye molecule to absorb two long-wavelength (λ_{CPM}) photons simultaneously, thus combining their energy in order to reach its excited state. Assuming a typical two-photon cross section (*8*) of $\delta = 10^{-58}$ m^4-s per photon with the above pulse parameters and the beam focused by a lens of numerical aperture $A \approx 1.4$, we calculated that an average incident laser power (p_0) of ~50 mW would saturate the fluorescence output at the limit of one absorbed photon pair per pulse per fluorophore (*9*). The fluorescence emission could be increased, however, if the pulse repetition frequency were increased to the inverse fluorescence

School of Applied and Engineering Physics, Department of Physics, Cornell University, Ithaca, NY 14853.

*Present address: IBM Forschungslaboratorium, Säumerstrasse 4, CH-8803 Rüschlikon, Switzerland.